applied sciences

MDPI

Review

Hepatic Steatosis Assessment Using Quantitative Ultrasound Parametric Imaging Based on Backscatter Envelope Statistics

Zhuhuang Zhou [1], Qiyu Zhang [1], Weiwei Wu [2], Shuicai Wu [1,*] and Po-Hsiang Tsui [3,4,5,*]

1 College of Life Science and Bioengineering, Beijing University of Technology, Beijing 100124, China; zhouzh@bjut.edu.cn (Z.Z.); zhangqiyu1994@163.com (Q.Z.)
2 College of Biomedical Engineering, Capital Medical University, Beijing 100054, China; wuweiwei8889@163.com
3 Department of Medical Imaging and Radiological Sciences, College of Medicine, Chang Gung University, Taoyuan 33302, Taiwan
4 Medical Imaging Research Center, Institute for Radiological Research, Chang Gung University and Chang Gung Memorial Hospital at Linkou, Taoyuan 33302, Taiwan
5 Department of Medical Imaging and Intervention, Chang Gung Memorial Hospital at Linkou, Taoyuan 33302, Taiwan
* Correspondence: wushuicai@bjut.edu.cn (S.W.); tsuiph@mail.cgu.edu.tw (P.-H.T.)

Received: 18 January 2019; Accepted: 7 February 2019; Published: 15 February 2019

Abstract: Hepatic steatosis is a key manifestation of non-alcoholic fatty liver disease (NAFLD). Early detection of hepatic steatosis is of critical importance. Currently, liver biopsy is the clinical golden standard for hepatic steatosis assessment. However, liver biopsy is invasive and associated with sampling errors. Ultrasound has been recommended as a first-line diagnostic test for the management of NAFLD. However, B-mode ultrasound is qualitative and can be affected by factors including image post-processing parameters. Quantitative ultrasound (QUS) aims to extract quantified acoustic parameters from the ultrasound backscattered signals for ultrasound tissue characterization and can be a complement to conventional B-mode ultrasound. QUS envelope statistics techniques, both statistical model-based and non-model-based, have shown potential for hepatic steatosis characterization. However, a state-of-the-art review of hepatic steatosis assessment using envelope statistics techniques is still lacking. In this paper, envelope statistics-based QUS parametric imaging techniques for characterizing hepatic steatosis are reviewed and discussed. The reviewed ultrasound envelope statistics parametric imaging techniques include acoustic structure quantification imaging, ultrasound Nakagami imaging, homodyned-K imaging, kurtosis imaging, and entropy imaging. Future developments are suggested.

Keywords: hepatic steatosis; noninvasive assessment; quantitative ultrasound; parametric imaging; envelope statistics; ultrasound tissue characterization

1. Introduction

Hepatic steatosis, a condition where excess fat accumulate within the hepatocytes, is a key manifestation of non-alcoholic fatty liver disease (NAFLD). With the growing epidemic of obesity, the incidence of NAFLD has significantly increased in the past decades, with a prevalence reported to be 6–35% (median 20%) worldwide [1]. NAFLD may progress to non-alcoholic steatohepatitis (NASH), causing chronic inflammation of the liver parenchyma, which may develop into a fibrosis, a cirrhosis, or a liver cancer. Therefore, early detection of hepatic steatosis is of critical importance.

Currently, liver biopsy is the clinical golden standard for hepatic steatosis assessment. However, liver biopsy is invasive and associated with sampling errors. Medical imaging has become a noninvasive alternative to liver biopsy; the modalities include computed tomography (CT), magnetic resonance (MR) spectroscopy, MR imaging, and ultrasound imaging [2]. MR spectroscopy-derived proton-density fat fraction (PDFF) is currently accepted as the noninvasive reference standard for hepatic steatosis quantification [2,3]. However, MR and CT are expensive with limited availability, and CT involves the use of radiation. Compared to CT and MR, ultrasound imaging has advantages of low cost, wide availability, and real-time capability [4–6]. Ultrasound has been recommended as a first-line diagnostic test for the management of NAFLD [7].

Ultrasound imaging involves a transducer transmitting ultrasound waves into a tissue being interrogated. The incident waves interact with the tissue and the transducer receives backscattered signals (Figure 1). B-mode (Brightness-mode) ultrasound imaging, which is based on the amplitude of the envelope of beamformed radiofrequency (RF) signals, is frequently used in clinical routine for the assessment of hepatic steatosis. Additionally, B-mode ultrasound image processing techniques, including deep learning [8,9], have been investigated for characterizing hepatic steatosis. However, B-mode ultrasound is qualitative and can be affected by factors including image post-processing parameters. Quantitative ultrasound (QUS) [10] aims to extract quantified acoustic parameters from the ultrasound backscattered signals for ultrasound tissue characterization. QUS has been explored for evaluating hepatic steatosis, including speed of sound [11,12], ultrasound attenuation [13,14], backscatter coefficient [14], and shear-wave dispersion [15].

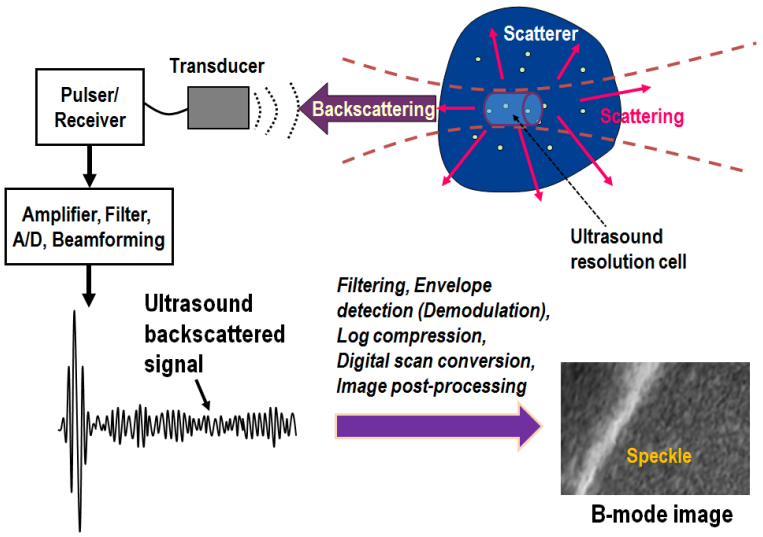

Figure 1. Ultrasound scattering and brightness mode (B-mode) image formation.

Acoustically, a liver tissue can be thought of as a collection of ultrasound scatterers [16]. The ultrasound backscattered signals are a spatial summation of the scattered waves contributed by each scatterer. QUS envelope statistics [17] extracts statistical information from the envelope of backscattered RF signals and is related to liver tissue microstructures. Envelope statistics techniques, both statistical model-based [18–20] and non-model-based [21,22], have shown potential for hepatic steatosis characterization. However, a state-of-the-art review of hepatic steatosis assessment using envelope statistics techniques is still lacking.

In this paper, envelope statistics–based QUS parametric imaging techniques for characterizing hepatic steatosis are reviewed and discussed. Future developments are also suggested. The remainder of this paper is arranged as follows. In Section 2, the algorithmic steps for ultrasound envelope statistics parametric imaging will be introduced. Then, statistical model-based and non-model-based ultrasound envelope statistics parametric imaging techniques for hepatic steatosis assessment will be

reviewed in Sections 3 and 4. A discussion on state-of-the-art techniques and future developments will be made in Section 5.

2. Ultrasound Envelope Statistics Parametric Imaging

Figure 2 illustrates the typical algorithmic steps for ultrasound envelope statistics parametric imaging. The ultrasound backscattered signals, or beamformed RF signals, are demodulated for envelope detection, with the Hilbert transform. Using the detected, uncompressed envelope, a computational kernel is conducted, which involves a sliding window moving throughout the envelope image. Each envelope statistics parameter is estimated using the envelope samples within the current sliding window. Then, a statistical parametric map is obtained. By performing digital scan conversion and color mapping to the statistical parametric map, an ultrasound envelope statistics parametric image is constructed. It should be noted that the B-mode ultrasound image is obtained by conducting log-compression and digital scan conversion to the detected envelope. Ultrasound envelope statistics parametric imaging can provide quantitative parametric information related to QUS envelope statistics, thus being a complement to conventional B-mode ultrasound imaging that offers qualitative structural information.

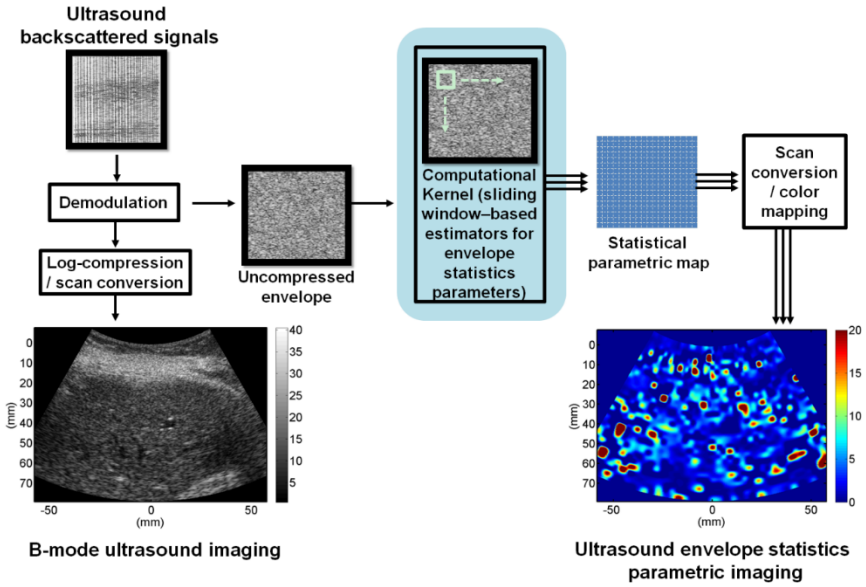

Figure 2. Typical algorithmic steps for ultrasound envelope statistics parametric imaging.

3. Statistical Model-Based Ultrasound Envelope Statistics Parametric Imaging Techniques

Ultrasound backscattered signals are essentially random signals. There is a correlation between the probability distribution pattern of the envelope of the backscattered signals and the tissue characteristics (Figure 3). If there are a large number of scatterers ($\geq$10) randomly distributed in the ultrasound resolution cell, the envelope statistics will obey Rayleigh distribution. In this case, the B-mode image speckle is called fully developed speckle. Considering the diversity of human tissue structure, the scatterer distribution in different tissues does not necessarily meet the conditions of fully developed speckle. Therefore, many researchers began to develop non-Rayleigh statistical models to describe envelope statistics. Among them, Nakagami and homodyned-K (HK) distributions are the two most important generalized models.

In this section, three kinds of statistical model-based ultrasound envelope statistics parametric imaging techniques for characterizing hepatic steatosis are reviewed: acoustic structure quantification (ASQ) imaging which uses the Rayleigh model, ultrasound Nakagami parametric imaging which uses the Nakagami model, and ultrasound HK parametric imaging which uses the HK model. The theories

of these statistical models and the parameter estimation methods are introduced, followed by the applications of statistical model-based ultrasound envelope statistics parametric imaging to hepatic steatosis assessment.

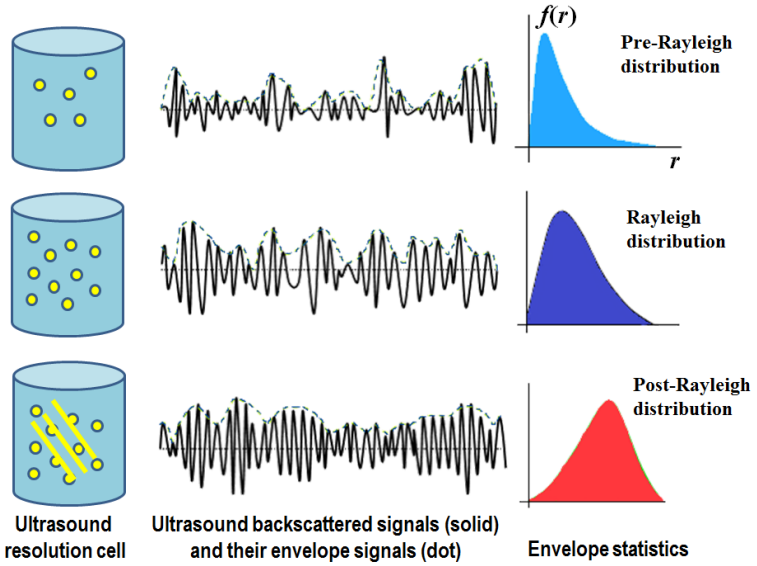

Figure 3. Rayleigh and non-Rayleigh distribution models for ultrasound backscatter envelope statistics.

3.1. Acoustic Structure Quantification Imaging

ASQ (Aplio XG; Toshiba Medical Systems, Otawara, Japan) is a novel ultrasound imaging modality for liver tissue characterization that measures the difference between the envelope statistics and the Rayleigh distribution. In ASQ, the envelopes are used to compute C_m^2, a statistical parameter for describing the backscattered statistics [23].

$$C_m^2 = \frac{\pi}{4-\pi}\frac{[E(r-E(r))]^2}{[E(r)]^2}, \quad (1)$$

where r denotes the envelope amplitude, and $E(.)$ is the expectation operator. Using the signals with amplitude $< \mu + 4\sigma$, where μ and σ denote the mean and standard deviation of the envelopes, respectively, the parameter C_m^2 is recalculated to be rC_m^2. Then, rC_m^2 is compared to the original C_m^2 to derive the focal disturbance ratio (FD ratio) [24].

The performance of ASQ imaging in assessing hepatic steatosis was investigated in some animal studies [18,24,25]. Using a rat model ($n = 32$), Lee et al. [18] showed that ASQ had a correlation $r = -0.90$ ($p < 0.001$) with MR spectroscopy measurements. Using a mouse model ($n = 9$), Kuroda et al. [24] reported that ASQ had a correlation $r = -0.72$ ($p = 0.0017$) with histopathology. Shen et al. [25] investigated ASQ and Nakagami imaging for characterizing hepatic steatosis, using a mouse model ($n = 24$); the reference standard was histopathology. They showed that both ASQ and Nakagami imaging techniques can distinguish normal and fatty livers.

However, the diagnostic value of using ASQ to quantify the degree of liver fat in the context of human hepatic steatosis remains questionable because of inconsistent findings. For example, Son et al. [26] demonstrated that the FD ratio had a correlation coefficient of -0.87 ($p < 0.001$) with MR spectroscopy measurements for 89 patients, whereas Karlas et al. [27] obtained a correlation coefficient of -0.43 ($p = 0.004$) with MR spectroscopy measurements for 70 patients. In addition to its inconsistent findings for fatty liver characterization, ASQ also results in different findings in liver fibrosis assessment [28]. Probably, the criteria used for rejecting signals and comparing C_m^2 and rC_m^2 in the ASQ algorithm are empirically determined [25], increasing the uncertainty in ASQ analysis.

3.2. Ultrasound Nakagami Imaging

The Nakagami statistical model was first introduced into the biomedical ultrasound field by Shankar [29]. The probability density function (PDF) of the Nakagami model is defined by [29]

$$f_{\mathrm{N}}(r) = \frac{2m^m r^{2m-1}}{\Gamma(m)\Omega^m} \exp\left(-\frac{m}{\Omega} r^2\right) U(r), \tag{2}$$

where $\Gamma(\cdot)$ and $U(\cdot)$ denote the gamma function and the unit step function, respectively; Ω is the scale parameter; m is the shape parameter. For $m < 1$, the envelope statistics is pre-Rayleigh distribution, meaning there are a small amount of scatterers (<10) randomly distributed in the ultrasound resolution cell. When $m = 1$, the envelope statistics becomes Rayleigh distribution, meaning there are many scatterers ($\geq$10) randomly distributed in the ultrasound resolution cell. When $m > 1$, the envelope statistics turns into post-Rayleigh distribution, meaning there are peridoic scatterers or local high-concentration scatterer aggregation, in addition to many scatterers ($\geq$10) randomly distributed in the ultrasound resolution cell (Figure 2). Therefore, the Nakagami distribution is a generalized statistical model for ultrasound backscattering.

The Nakagami distribution can be regarded as an approximation of the HK model [10]. Because of its low computational complexity, the Nakagami distribution has become the most widely used statistical model in the field of medical ultrasound; typical applications of Nakagami model have been summarized by Tsui et al. [30]. The estimation methods of Nakagami m parameter mainly include moment-based estimators [19,31,32] and maximum likelihood estimators [30,32,33]. It should be noted that window-modulated compounding (WMC) Nakagami imaging was proposed by Tsui et al. [34] for simultaneous improvement of image resolution and smoothness of Nakagami images.

Animal models [19,31] and clinical studies [35] have shown that the m parameter estimated by the moment-based estimators increases with the increasing severity of hepatic steatosis. Using a rat model (n = 24), Ho et al. [31] reported that ultrasound Nakagami imaging is well correlated with the amount of the total cholesterol (r = 0.86; $p < 0.0001$) and triglyceride (r = 0.79; $p < 0.0001$) in the liver tissue, respectively. Zhou et al. [19] investigated three-dimensional WMC Nakagami imaging for characterizing hepatic steatosis in a rat model (n = 18); the Nakagami m parameter had a correlation r^2 = 0.94 with the methionine-choline-deficient diet weeks. Wan et al. [35] investigated ultrasound Nakagami imaging for assessing hepatic steatosis of 107 patients; the reference standard was an ultrasonographic scoring system [36]. A correlation r = 0.84 ($p < 0.0001$) was reported.

3.3. Ultatrasound Homodyned-K Imaging

The PDF of the HK model is defined by [37]

$$f_{\mathrm{H}}(r) = r \int_0^\infty x J_0(sx) J_0(rx) \left(1 + (x^2\sigma^2)/(2\mu)\right)^{-\mu} dx, \tag{3}$$

where $J_0(\cdot)$ is the zeroth-order Bessel function of the first kind; s^2 is the coherent signal energy; σ^2 denotes the diffuse signal energy; μ denotes the effective number of scatterers per resolution cell; the derived parameter $k = s/\sigma$ represents the ratio of the coherent to diffuse signal.

The HK distribution is considered as a statistical model of ultrasound backscattered signals whose parameters have a physical meaning [10,38]. However, the application of the HK model has been limited due to the analytical complexity in estimating the parameters. Currently, there are moment-based estimators [37,39–41] and numerical methods [42] for estimating HK parameters. Moment-based estimators include (i) the estimator that uses the signal-to-noise ratio (SNR) and the skewness based on the first three integer moments of the intensity, which is the square of the envelope (this method is termed "FTM") [37,39], (ii) a level-curve method that uses the SNR, skewness, and kurtosis based on the fractional moments of the envelope (this method is termed "RSK") [40], and (iii)

an estimation method based on the first moment of the intensity and two log-moments, namely X- and U-statistics (this method is termed "XU") [41].

The HK model has been applied to characterizing cell pellet biophantoms [43], tissue phantom heated by focused ultrasound [44], reperfused infarcted porcine myocardium in vivo [45], mice breast cancer in vivo [46], human breast lesions in vivo [47,48], response of advanced human breast cancer to neoadjuvant chemotherapy in vivo [49], cancerous human lymph nodes ex vivo [50], porcine red blood cell aggregation ex vivo [51], human carotid artery plaque in vivo [52], human skin ulcer ex vivo [53], nonalcoholic steatohepatitis of rats in vivo [54], and hepatic steatosis of rabbit livers ex vivo [55] and rat livers in vivo [20].

Using a rat model, Ghoshal et al. [55] demonstrated that there is a significant increase in the HK μ parameter with increasing fat content in the liver samples. Using a rat model, Fang et al. [20] reported that the μ parameter increased monotonically as the steatosis stage increased. The area under the receiver operating characteristic curve (AUC) was 0.947, 0.914, and 0.813 for $\geq$mild, $\geq$moderate, and $\geq$severe, respectively. However, the feasibility of the HK model in detecting human hepatic steatosis in vivo remains unknown.

4. Non-Model-Based Ultrasound Envelope Statistics Parametric Imaging Techniques

In this section, two kinds of non-model-based ultrasound envelope statistics parametric imaging techniques for characterizing hepatic steatosis are reviewed: ultrasound kurtosis imaging and ultrasound entropy imaging.

4.1. Ultrasound Kurtosis Imaging

Kurtosis K is a parameter of the shape of a probability distribution and is defined as the normalized fourth moment of envelope amplitude r [56]:

$$K = \frac{E[(r - E(r))^4]}{\left(E[(r - E(r))^2]\right)^2}. \tag{4}$$

The kurtosis is a measure of the peakedness of the probability distribution. Kurtosis $K = 3$ represents that the probability distribution of the backscatter envelope is a Gaussian distribution. When K is larger and smaller than 3, the probability distribution of the backscatter envelope is leptokurtic (slender) and platykurtic (broad), respectively.

Ma et al. [21] investigated ultrasound kurtosis imaging for characterizing hepatic steatosis of 107 patients. The reference standard was an ultrasonographic scoring system [36]. The kurtosis decreased from 5.41 ± 0.89 to 3.68 ± 0.12 with increasing the score of fatty liver from 0 (normal) to 3 (severe), indicating that hepatic steatosis reduces the degree of peakedness of backscatter statistics. The AUC was 0.92, 0.90, and 0.82 for $\geq$mild, $\geq$moderate, and $\geq$severe, respectively. It was suggested that ultrasound kurtosis imaging may be useful in designing computer-aided diagnosis tools to assist physicians in early detection of hepatic steatosis.

4.2. Ultrasound Entropy Imaging

The information-theoretic entropy was first introduced into the biomedical ultrasound field by Hughes [57]. Shannon entropy H is defined by [58]

$$H \equiv -\int_{r_{\min}}^{r_{\max}} w(r) \log_2[w(r)] dr, \tag{5}$$

where $r_{\min}$ and $r_{\max}$ are the minimum and maximum envelope amplitudes, respectively; $w(r)$ is the PDF of envelope amplitude r. Shannon entropy reflects the uncertainty of random signals. A larger value

of Shannon entropy indicates a greater uncertainty, representing that the ultrasound backscattered signals change from regular to random and even complex states [58].

Clinical studies demonstrated that Shannon entropy increases with increasing severity of hepatic steatosis [22,59,60]. Tsui et al. [59] investigated ultrasound entropy imaging for assessing hepatic steatosis of 107 patients, using an ultrasonographic scoring system [36] as the reference standard. A correlation $r = 0.63$ ($p < 0.0001$) was reported. Lin et al. [60] assessed hepatic steatosis of 394 patients with ultrasound entropy and ASQ imaging; the reference standard was an ultrasonographic fatty liver indicator [61]. Correlations of $r = 0.713$ ($p < 0.0001$) and $r = –0.630$ ($p < 0.0001$) were reported for entropy and ASQ imaging, respectively. Zhou et al. [22] investigated small-window entropy imaging for characterizing hepatic steatosis in liver donors ($n = 53$) and patients ($n = 142$); the reference standards were MR spectroscopy and histopathology for liver donors and patients, respectively. A correlation $r = 0.74$ with MR spectroscopy measurements was reported. For liver patients, the AUC was 0.80, 0.90, and 0.89 for ≥mild, ≥moderate, and ≥severe, respectively.

5. Discussion

Envelope statistics is an important group of QUS parameters for ultrasound tissue characterization. Ultrasound envelope statistics parametric imaging has potential in assessing hepatic steatosis. As this imaging method is based on ultrasound backscattered signals, it is compatible with a conventional pulse-echo ultrasound imaging framework. To the best of our knowledge, this paper is the first to review the state-of-the-art ultrasound envelope statistics parametric imaging techniques for characterizing hepatic steatosis.

Table 1 provides a summary of ultrasound envelope statistics parametric imaging techniques for hepatic steatosis assessment, in terms of study type, case number, reference standard, and performance. The reviewed ultrasound envelope statistics parametric imaging techniques include ASQ imaging, ultrasound Nakagami imaging, HK imaging, kurtosis imaging, and entropy imaging. ASQ imaging, Nakagami imaging, and HK imaging are based on statistical models, while kurtosis imaging and entropy imaging are not. ASQ imaging, Nakagami imaging, kurtosis imaging, and entropy imaging have been applied to clinical studies, but HK imaging have not. The performance of HK imaging in assessing human hepatic steatosis should be explored in future developments.

Statistical model-based and non-model-based ultrasound envelope statistics parametric imaging techniques are compared as follows. A prerequisite for using statistical models describing the statistical properties of ultrasound backscattered signals is that the ultrasound backscattered data must conform to the used distribution [22,58]. This may not always be satisfied because of the differing signal detection and processing hardware and software designs among different ultrasound imaging systems. In this sense, non-model-based ultrasound envelope statistics parametric imaging, which can be computed using any data regardless of the distribution model, may have more flexibility in tissue characterization [22].

Table 2 compares the advantages and limitations of different ultrasound envelope statistics parametric imaging techniques. ASQ imaging has been commercialized with higher availability, but inconsistent findings for characterizing human hepatic steatosis have been reported [26,27]. Ultrasound Nakagami imaging has low computational complexity, but the m parameter plateaus around 1 for higher scatterer concentrations [43]. Ultrasound HK imaging is based on parameters of a physical meaning, but the analytical complexity for estimating HK parameters is high. Ultrasound kurtosis imaging is easy to implement, but it needs further validation in hepatic steatosis assessment. Ultrasound entropy imaging can use a small sliding window, thus allowing a small-window, high-resolution imaging, but the dynamic range of the Shannon entropy value is limited [22]. The limitations may be overcome in future developments.

Table 1. Summary of ultrasound envelope statistics parametric imaging techniques for hepatic steatosis assessment.

Authors	Technique	Study	#	Ref. Std.	Performance
Kuroda, 2012 [24]	ASQ imaging	Mouse model study	9	Histopathology	$r = -0.72$ ($p = 0.0017$)
Shen, 2016 [25]	ASQ imaging Ultrasound Nakagami imaging	Mouse model study	24	Histopathology	Both techniques can distinguish normal and fatty livers
Lee, 2017 [18]	ASQ imaging	Rat model study	32	MR spectroscopy	$r = -0.90$ ($p < 0.001$)
Karlas, 2015 [27]	ASQ imaging	Clinical study	70	MR spectroscopy	$r = -0.43$ ($p = 0.004$)
Son, 2016 [26]	ASQ imaging	Clinical study	89	MR spectroscopy	$r = -0.87$ ($p < 0.001$)
Ho, 2013 [31]	Ultrasound Nakagami imaging	Rat model study	24	Histopathology	$r = 0.86$ ($p < 0.001$)
Wan, 2015 [35]	Ultrasound Nakagami imaging	Clinical study	107	Ultrasonographic scoring system	$r = 0.84$ ($p < 0.0001$)
Zhou, 2018 [19]	Ultrasound Nakagami imaging	Rat model study	18	-	$r^2 = 0.94$
Ghoshal, 2012 [55]	Ultrasound HK imaging	Rabbit model study	14	Histopathology	Significant increase in the μ parameter
Fang, 2018 [20]	Ultrasound HK imaging	Rat model study	36	Histopathology	AUC = 0.947 (≥mild), 0.914 (≥moderate), 0.813 (≥severe)
Ma, 2016 [21]	Ultrasound kurtosis imaging	Clinical study	107	Ultrasonographic scoring system	AUC = 0.92 (≥mild), 0.90 (≥moderate), 0.82 (≥severe)
Tsui, 2016 [59]	Ultrasound entropy imaging	Clinical study	107	Ultrasonographic scoring system	$r = 0.63$ ($p < 0.0001$)
Lin, 2018 [60]	Ultrasound entropy imaging ASQ imaging	Clinical study	394	Ultrasonographic fatty liver indicator	$r = 0.713$ ($p < 0.0001$) $r = -0.630$ ($p < 0.0001$)
Zhou, 2018 [22]	Ultrasound entropy imaging	Clinical study	53 142	MR spectroscopy Histopathology	$r = 0.74$ ($p < 0.0001$) AUC = 0.80 (≥mild), 0.90 (≥moderate), 0.89 (≥severe)

Ref. std.: reference standard; ASQ: acoustic structure quantification; HK: homodyned-K; MR: magnetic resonance; AUC: area under the receiver operating characteristic curve.

Table 2. Comparison of ultrasound envelope statistics parametric imaging techniques.

Technique	Advantage	Limitation
ASQ imaging	Have been commercialized	Inconsistent findings for characterizing human hepatic steatosis
Ultrasound Nakagami imaging	Low computational complexity	The m parameter plateaus around 1 for higher scatterer concentrations
Ultrasound HK imaging	Have a physical meaning	High analytical complexity
Ultrasound kurtosis imaging	Easy to compute	Need further validation
Ultrasound entropy imaging	Allow a small-window (high-resolution) imaging	The dynamic range of Shannon entropy is limited

ASQ: acoustic structure quantification; HK: homodyned-K.

There are some studies comparing the performance of different ultrasound envelope statistics parametric imaging techniques in assessing hepatic steatosis. Shen et al. [25] compared Nakagami with ASQ imaging and showed that ASQ may be more stable and provides higher sensitivity than Nakagami imaging. Zhou et al. [22] demonstrated that entropy imaging yields a better performance than Nakagami imaging, for both liver donors and patients. Lin et al. [60] compared entropy imaging with ASQ imaging and showed that entropy imaging outperforms ASQ imaging. More comparisons

between different ultrasound envelope statistics parametric imaging techniques are expected in future developments.

The size of the sliding windows (Figure 2) has an impact on ultrasound envelope statistics parametric imaging. Using a large window to construct a parametric image results in stable parameter estimation and enhanced image smoothness. By contrast, a small window (corresponding to a small spatial scale) enables the achievement of enhanced envelope statistics parametric image resolution. The effects of the window size on envelope statistics parametric imaging of hepatic steatosis should be investigated in future developments.

The estimators for estimating envelope statistics parameters also can affect the performance of ultrasound envelope statistics parametric imaging of hepatic steatosis. Different estimators should be compared, and new estimators can be developed. In addition, new envelope statistics parameters and associated parametric imaging methods can be explored in future developments.

It would be interesting to investigate the relationship of envelope statistics to other QUS parameters such as tissue elasticity, so that a better characterization of tissue microstructures can be realized. Additionally, combination of different envelope statistics parametric imaging techniques, and combination of envelope statistics parametric imaging techniques with other QUS imaging techniques may be explored in future developments, in order to improve the performance of hepatic steatosis characterization. For instance, a recent study combined HK imaging with ultrasound elastography for a better characterization of nonalcoholic steatohepatitis of a rat model [54].

Investigating three-dimensional envelope statistics parametric imaging can provide more complete information and clues related to hepatic steatosis. Compared with one-dimensional or two-dimensional envelope statistics parametric imaging, three-dimensional envelope statistics parametric imaging can offer an enhanced characterization of hepatic steatosis, which involves the construction of the three-dimensional envelope statistics parametric image. Currently, only three-dimensional Nakagami imaging has been proposed for hepatic steatosis assessment [19]. Three-dimensional parametric imaging based on other envelope statistics parameters can be explored for characterizing hepatic steatosis in future developments.

Author Contributions: Conceptualization, Z.Z., S.W., and P.-H.T.; investigation, Z.Z., Q.Z., and W.W.; writing—original draft preparation, Z.Z., Q.Z., and W.W.; writing—review and editing, S.W. and P.-H.T.; project administration, S.W. and P.-H.T.; funding acquisition, Z.Z., W.W., and S.W.

Funding: This work was supported in part by the National Natural Science Foundation of China (Grant Nos. 11804013, 61871005, 71661167001, and 61801312), the Beijing Natural Science Foundation (Grant No. 4184081), the International Research Cooperation Seed Fund of Beijing University of Technology (Grant No. 2018A15), the Basic Research Fund of Beijing University of Technology, and the Intelligent Physiological Measurement and Clinical Translation, Beijing International Base for Scientific and Technological Cooperation.

Conflicts of Interest: The authors declare no conflict of interest. The funders had no role in the design of the study; in the collection, analyses, or interpretation of data; in the writing of the manuscript, or in the decision to publish the results.

References

1. Bellentani, S. The epidemiology of non-alcoholic fatty liver disease. *Liver Int.* **2017**, *37*, 81–84. [CrossRef] [PubMed]
2. Zhang, Y.N.; Fowler, K.J.; Hamilton, G.; Cui, J.Y.; Sy, E.Z.; Balanay, M.; Hooker, J.C.; Szeverenyi, N.; Sirlin, C.B. Liver fat imaging-a clinical overview of ultrasound, CT, and MR imaging. *Br. J. Radiol.* **2018**, *91*, 20170959. [CrossRef] [PubMed]
3. Kramer, H.; Pickhardt, P.J.; Kliewer, M.A.; Hernando, D.; Chen, G.H.; Zagzebski, J.A.; Reeder, S.B. Accuracy of liver fat quantification with advanced CT, MRI, and ultrasound techniques: Prospective comparison with MR spectroscopy. *AJR Am. J. Roentgenol.* **2017**, *208*, 92–100. [CrossRef] [PubMed]
4. Huang, Q.; Wu, B.; Lan, J.; Li, X. Fully automatic three-dimensional ultrasound imaging based on conventional B-scan. *IEEE Trans. Biomed. Circuits Syst.* **2018**, *12*, 426–436. [CrossRef] [PubMed]

5. Huang, Q.; Zeng, Z.; Li, X. 2.5-D extended field-of-view ultrasound. *IEEE Trans. Med. Imaging* **2018**, *37*, 851–859. [CrossRef] [PubMed]
6. Huang, Q.; Lan, J.; Li, X. Robotic arm based automatic ultrasound scanning for three-dimensional imaging. *IEEE Trans. Industr. Inform.* **2019**, *15*, 1173–1182. [CrossRef]
7. European Association for the Study of the Liver; European Association for the Study of Diabetes; European Association for the Study of Obesity. EASL-EASD-EASO Clinical Practice Guidelines for the management of non-alcoholic fatty liver disease. *J. Hepatol.* **2016**, *64*, 1388–1402. [CrossRef] [PubMed]
8. Biswas, M.; Kuppili, V.; Edla, D.R.; Suri, H.S.; Saba, L.; Marinhoe, R.T.; Sanches, J.M.; Suri, J.S. Symtosis: A liver ultrasound tissue characterization and risk stratification in optimized deep learning paradigm. *Comput. Methods Programs Biomed.* **2018**, *155*, 165–177. [CrossRef]
9. Byra, M.; Styczynski, G.; Szmigielski, C.; Kalinowski, P.; Michalowski, L.; Paluszkiewicz, R.; Ziarkiewicz-Wroblewska, B.; Zieniewicz, K.; Sobieraj, P.; Nowicki, A. Transfer learning with deep convolutional neural network for liver steatosis assessment in ultrasound images. *Int. J. Comput. Assist. Radiol. Surg.* **2018**, *13*, 1895–1903. [CrossRef]
10. Mamou, J.; Oelze, M.L. *Quantitative Ultrasound in Soft Tissues*; Springer: Heidelberg, Germany, 2013; pp. 21–35.
11. Dioguardi Burgio, M.; Imbault, M.; Ronot, M.; Faccinetto, A.; Van Beers, B.E.; Rautou, P.E.; Castera, L.; Gennisson, J.L.; Tanter, M.; Vilgrain, V. Ultrasonic adaptive sound speed estimation for the diagnosis and quantification of hepatic steatosis: A pilot study. *Ultraschall Med.* **2019**, in press. [CrossRef]
12. Zubajlo, R.E.; Benjamin, A.; Grajo, J.R.; Kaliannan, K.; Kang, J.X.; Bhan, A.K.; Thomenius, K.E.; Anthony, B.W.; Dhyani, M.; Samir, A.E. Experimental validation of longitudinal speed of sound estimates in the diagnosis of hepatic steatosis (part II). *Ultrasound Med. Biol.* **2018**, *44*, 2749–2758. [CrossRef] [PubMed]
13. Fujiwara, Y.; Kuroda, H.; Abe, T.; Ishida, K.; Oguri, T.; Noguchi, S.; Sugai, T.; Kamiyama, N.; Takikawa, Y. The B-mode image-guided ultrasound attenuation parameter accurately detects hepatic steatosis in chronic liver disease. *Ultrasound Med. Biol.* **2018**, *44*, 2223–2232. [CrossRef] [PubMed]
14. Han, A.; Andre, M.P.; Deiranieh, L.; Housman, E.; Erdman, J.W., Jr.; Loomba, R.; Sirlin, C.B.; O'Brien, W.D., Jr. Repeatability and reproducibility of the ultrasonic attenuation coefficient and backscatter coefficient measured in the right lobe of the liver in adults with known or suspected nonalcoholic fatty liver disease. *J. Ultrasound Med.* **2018**, *37*, 1913–1927. [CrossRef] [PubMed]
15. Ozturk, A.; Grajo, J.R.; Gee, M.S.; Benjamin, A.; Zubajlo, R.E.; Thomenius, K.E.; Anthony, B.W.; Samir, A.E.; Dhyani, M. Quantitative hepatic fat quantification in non-alcoholic fatty liver disease using ultrasound-based techniques: A review of literature and their diagnostic performance. *Ultrasound Med. Biol.* **2018**, *44*, 2461–2475. [CrossRef] [PubMed]
16. Zhou, Z.; Wu, W.; Wu, S.; Jia, K.; Tsui, P.H. A review of ultrasound tissue characterization with mean scatterer spacing. *Ultrason. Imaging* **2017**, *39*, 263–282. [CrossRef] [PubMed]
17. Oelze, M.L.; Mamou, J. Review of quantitative ultrasound envelope statistics and backscatter coefficient imaging and contributions to diagnostic ultrasound. *IEEE Trans. Ultrason. Ferroelectr. Freq. Control* **2016**, *63*, 336–351. [CrossRef] [PubMed]
18. Lee, D.H.; Lee, J.Y.; Lee, K.B.; Han, J.K. Evaluation of hepatic steatosis by using acoustic structure quantification US in a rat model: Comparison with pathologic examination and MR spectroscopy. *Radiology* **2017**, *285*, 445–453. [CrossRef]
19. Zhou, Z.; Wu, S.; Lin, M.Y.; Fang, J.; Liu, H.L.; Tsui, P.H. Three-dimensional visualization of ultrasound backscatter statistics by window-modulated compounding Nakagami imaging. *Ultrason. Imaging* **2018**, *40*, 171–189. [CrossRef]
20. Fang, J.; Zhou, Z.; Chang, N.F.; Wan, Y.L.; Tsui, P.H. Ultrasound parametric imaging of hepatic steatosis using the homodyned-K distribution: An animal study. *Ultrasonics* **2018**, *87*, 91–102. [CrossRef]
21. Ma, H.Y.; Zhou, Z.; Wu, S.; Wan, Y.L.; Tsui, P.H. A computer-aided diagnosis scheme for detection of fatty liver in vivo based on ultrasound kurtosis imaging. *J. Med. Syst.* **2016**, *40*, 33. [CrossRef]
22. Zhou, Z.; Tai, D.I.; Wan, Y.L.; Tseng, J.H.; Lin, Y.R.; Wu, S.; Yang, K.C.; Liao, Y.Y.; Yeh, C.K.; Tsui, P.H. Hepatic steatosis assessment with ultrasound small-window entropy imaging. *Ultrasound Med. Biol.* **2018**, *44*, 1327–1340. [CrossRef] [PubMed]
23. Toyoda, H.; Kumada, T.; Kamiyama, N.; Shiraki, K.; Takase, K.; Yamaguchi, T.; Hachiya, H. B-mode ultrasound with algorithm based on statistical analysis of signals: Evaluation of liver fibrosis in patients with chronic hepatitis C. *AJR Am. J. Roentgenol.* **2009**, *193*, 1037–1043. [CrossRef] [PubMed]

24. Kuroda, H.; Kakisaka, K.; Kamiyama, N.; Oikawa, T.; Onodera, M.; Sawara, K.; Oikawa, K.; Endo, R.; Takikawa, Y.; Suzuki, K. Non-invasive determination of hepatic steatosis by acoustic structure quantification from ultrasound echo amplitude. *World J. Gastroenterol.* **2012**, *18*, 3889–3895. [CrossRef] [PubMed]
25. Shen, C.C.; Yu, S.C.; Liu, C.Y. Using high-frequency ultrasound statistical scattering model to assess nonalcoholic fatty liver disease (NAFLD) in mice. In Proceedings of the 39th International Conference on Telecommunications and Signal Processing (TSP), Vienna, Austria, 27–29 June 2016; pp. 379–382.
26. Son, J.Y.; Lee, J.Y.; Yi, N.J.; Lee, K.W.; Suh, K.S.; Kim, K.G.; Lee, J.M.; Han, J.K.; Choi, B.I. Hepatic steatosis: Assessment with acoustic structure quantification of US imaging. *Radiology* **2016**, *278*, 257–264. [CrossRef] [PubMed]
27. Karlas, T.; Berger, J.; Garnov, N.; Lindner, F.; Busse, H.; Linder, N.; Schaudinn, A.; Relke, B.; Chakaroun, R.; Troltzsch, M.; et al. Estimating steatosis and fibrosis: Comparison of acoustic structure quantification with established techniques. *World J. Gastroenterol.* **2015**, *21*, 4894–4902. [CrossRef] [PubMed]
28. Kramer, C.; Jaspers, N.; Nierhoff, D.; Kuhr, K.; Bowe, A.; Goeser, T.; Michels, G. Acoustic structure quantification ultrasound software proves imprecise in assessing liver fibrosis or cirrhosis in parenchymal liver diseases. *Ultrasound Med. Biol.* **2014**, *40*, 2811–2818. [CrossRef] [PubMed]
29. Shankar, P.M. A general statistical model for ultrasonic backscattering from tissues. *IEEE Trans. Ultrason. Ferroelectr. Freq. Control* **2000**, *47*, 727–736. [CrossRef]
30. Tsui, P.H.; Wan, Y.L.; Tai, D.I.; Shu, Y.C. Effects of estimators on ultrasound Nakagami imaging in visualizing the change in the backscattered statistics from a Rayleigh distribution to a Pre-Rayleigh distribution. *Ultrasound Med. Biol.* **2015**, *41*, 2240–2251. [CrossRef]
31. Ho, M.C.; Lee, Y.H.; Jeng, Y.M.; Chen, C.N.; Chang, K.J.; Tsui, P.H. Relationship between ultrasound backscattered statistics and the concentration of fatty droplets in livers: An animal study. *PLoS ONE* **2013**, *8*, e63543. [CrossRef]
32. Lin, J.J.; Cheng, J.Y.; Huang, L.F.; Lin, Y.H.; Wan, Y.L.; Tsui, P.H. Detecting changes in ultrasound backscattered statistics by using Nakagami parameters: Comparisons of moment-based and maximum likelihood estimators. *Ultrasonics* **2017**, *77*, 133–143. [CrossRef]
33. Han, M.; Wan, J.; Zhao, Y.; Zhou, X.; Wan, M. Nakagami-m parametric imaging for atherosclerotic plaque characterization using the coarse-to-fine method. *Ultrasound Med. Biol.* **2017**, *43*, 1275–1289. [CrossRef] [PubMed]
34. Tsui, P.H.; Ma, H.Y.; Zhou, Z.; Ho, M.C.; Lee, Y.H. Window-modulated compounding Nakagami imaging for ultrasound tissue characterization. *Ultrasonics* **2014**, *54*, 1448–1459. [CrossRef] [PubMed]
35. Wan, Y.L.; Tai, D.I.; Ma, H.Y.; Chiang, B.H.; Chen, C.K.; Tsui, P.H. Effects of fatty infiltration in human livers on the backscattered statistics of ultrasound imaging. *Proc. Inst. Mech. Eng. H* **2015**, *229*, 419–428. [CrossRef] [PubMed]
36. Chan, D.F.; Li, A.M.; Chu, W.C.; Chan, M.H.; Wong, E.M.; Liu, E.K.; Chan, I.H.; Yin, J.; Lam, C.W.; Fok, T.F.; et al. Hepatic steatosis in obese Chinese children. *Int. J. Obes. Relat. Metab. Disord.* **2004**, *28*, 1257–1263. [CrossRef] [PubMed]
37. Dutt, V.; Greenleaf, J.F. Ultrasound echo envelope analysis using a homodyned K distribution signal model. *Ultrason. Imaging* **1994**, *16*, 265–287. [CrossRef] [PubMed]
38. Destrempes, F.; Cloutier, G. A critical review and uniformized representation of statistical distributions modeling the ultrasound echo envelope. *Ultrasound Med. Biol.* **2010**, *36*, 1037–1051. [CrossRef] [PubMed]
39. Prager, R.W.; Gee, A.H.; Treece, G.M.; Berman, L.H. Decompression and speckle detection for ultrasound images using the homodyned K-distribution. *Pattern Recognit. Lett.* **2003**, *24*, 705–713. [CrossRef]
40. Hruska, D.P.; Oelze, M.L. Improved parameter estimates based on the homodyned K distribution. *IEEE Trans. Ultrason. Ferroelectr. Freq. Control* **2009**, *56*, 2471–2481. [CrossRef]
41. Destrempes, F.; Poree, J.; Cloutier, G. Estimation method of the homodyned K-distribution based on the mean intensity and two log-moments. *SIAM J. Imaging Sci.* **2013**, *6*, 1499–1530. [CrossRef]
42. Hu, X.; Zhang, Y.; Deng, L.; Cai, G.; Zhang, Q.; Zhou, Y.; Zhang, K.; Zhang, J. Assessment of homodyned K distribution modeling ultrasonic speckles from scatterers with varying spatial organizations. *J. Healthc. Eng.* **2017**, *2017*, 8154780. [CrossRef]
43. Cristea, A.; Franceschini, E.; Lin, F.; Mamou, J.; Cachard, C.; Basset, O. Quantitative characterization of concentrated cell pellet biophantoms using statistical models for the ultrasound echo envelope. *Phys. Procedia* **2015**, *70*, 1091–1095. [CrossRef]

44. Byra, M.; Kruglenko, E.; Gambin, B.; Nowicki, A. Temperature monitoring during focused ultrasound treatment by means of the homodyned K distribution. *Acta Phys. Pol. A* **2017**, *131*, 1525–1528. [CrossRef]
45. Hao, X.; Bruce, C.J.; Pislaru, C.; Greenleaf, J.F. Characterization of reperfused infarcted myocardium from high-frequency intracardiac ultrasound imaging using homodyned K distribution. *IEEE Trans. Ultrason. Ferroelectr. Freq. Control* **2002**, *49*, 1530–1542.
46. Oelze, M.L.; O'Brien, W.D., Jr.; Zachary, J.F. Quantitative ultrasound assessment of breast cancer using a multiparameter approach. In Proceedings of the 2007 IEEE International Ultrasonics Symposium, New York, NY, USA, 28–31 October 2007; pp. 981–984.
47. Trop, I.; Destrempes, F.; El Khoury, M.; Robidoux, A.; Gaboury, L.; Allard, L.; Chayer, B.; Cloutier, G. The added value of statistical modeling of backscatter properties in the management of breast lesions at US. *Radiology* **2015**, *275*, 666–674. [CrossRef] [PubMed]
48. Byra, M.; Nowicki, A.; Wroblewska-Piotrzkowska, H.; Dobruch-Sobczak, K. Classification of breast lesions using segmented quantitative ultrasound maps of homodyned K distribution parameters. *Med. Phys.* **2016**, *43*, 5561–5569. [CrossRef] [PubMed]
49. Dobruch-Sobczak, K.; Piotrzkowska-Wróblewska, H.; Klimoda, Z.; Karwat, P.; Litniewski, J.; Roszkowska-Purska, K.; Markiewicz-Grodzicka, E. Quantitative ultrasound parameters assessment of advanced breast cancer in evaluation the response to neoadjuvant chemotherapy. *Eur. J. Cancer* **2018**, *92*, S149–S150. [CrossRef]
50. Mamou, J.; Coron, A.; Oelze, M.L.; Saegusa-Beecroft, E.; Hata, M.; Lee, P.; Machi, J.; Yanagihara, E.; Laugier, P.; Feleppa, E.J. Three-dimensional high-frequency backscatter and envelope quantification of cancerous human lymph nodes. *Ultrasound Med. Biol.* **2011**, *37*, 345–357. [CrossRef]
51. Destrempes, F.; Franceschini, E.; Yu, F.T.; Cloutier, G. Unifying concepts of statistical and spectral quantitative ultrasound techniques. *IEEE Trans. Med. Imaging* **2016**, *35*, 488–500. [CrossRef]
52. Roy-Cardinal, M.H.; Destrempes, F.; Soulez, G.; Cloutier, G. Assessment of carotid artery plaque components with machine learning classification using homodyned-K parametric maps and elastograms. *IEEE Trans. Ultrason. Ferroelectr. Freq. Control* **2019**, in press. [CrossRef]
53. Omura, M.; Yoshida, K.; Akita, S.; Yamaguchi, T. Verification of echo amplitude envelope analysis method in skin tissues for quantitative follow-up of healing ulcers. *Jpn. J. Appl. Phys.* **2018**, *57*, 07LF15. [CrossRef]
54. Tang, A.; Destrempes, F.; Kazemirad, S.; Garcia-Duitama, J.; Nguyen, B.N.; Cloutier, G. Quantitative ultrasound and machine learning for assessment of steatohepatitis in a rat model. *Eur. Radiol.* **2019**, in press. [CrossRef] [PubMed]
55. Ghoshal, G.; Lavarello, R.J.; Kemmerer, J.P.; Miller, R.J.; Oelze, M.L. Ex vivo study of quantitative ultrasound parameters in fatty rabbit livers. *Ultrasound Med. Biol.* **2012**, *38*, 2238–2248. [CrossRef] [PubMed]
56. Kuc, R. Ultrasonic tissue characterization using kurtosis. *IEEE Trans. Ultrason. Ferroelectr. Freq. Control* **1986**, *33*, 273–279. [CrossRef] [PubMed]
57. Hughes, M.S. Analysis of digitized waveforms using Shannon entropy. *J. Acoust. Soc. Am.* **1993**, *93*, 892–906. [CrossRef]
58. Zhou, Z.; Huang, C.C.; Shung, K.K.; Tsui, P.H.; Fang, J.; Ma, H.Y.; Wu, S.; Lin, C.C. Entropic imaging of cataract lens: An in vitro study. *PLoS ONE* **2014**, *9*, e96195. [CrossRef] [PubMed]
59. Tsui, P.H.; Wan, Y.L. Effects of fatty infiltration of the liver on the Shannon entropy of ultrasound backscattered signals. *Entropy* **2016**, *18*, 341. [CrossRef]
60. Lin, Y.H.; Liao, Y.Y.; Yeh, C.K.; Yang, K.C.; Tsui, P.H. Ultrasound entropy imaging of nonalcoholic fatty liver disease: Association with metabolic syndrome. *Entropy* **2018**, *20*, 893. [CrossRef]
61. Ballestri, S.; Lonardo, A.; Romagnoli, D.; Carulli, L.; Losi, L.; Day, C.P.; Loria, P. Ultrasonographic fatty liver indicator, a novel score which rules out NASH and is correlated with metabolic parameters in NAFLD. *Liver Int.* **2012**, *32*, 1242–1252. [CrossRef]